Journal of Marine Science and Engineering

MDPI

Article

On Cubic Spudcan Deep Penetration in Dense Sand Overlying Non-Uniform Clay

Jun Zhao [1,*], Yang Zhang [2] and Luyu Liu [3]

[1] Department of Offshore Oil and Gas Engineering, College of Petroleum Engineering, Xi'an Shiyou University, Xi'an 710065, China
[2] Department of Naval Architecture and Ocean Engineering, Ulsan Ship and Ocean College, Ludong University, Yantai 264000, China
[3] Yantai CIMC Blue Ocean Technology Co., Ltd., Yantai 264000, China
* Correspondence: junzhao@xsyu.edu.cn

Abstract: Installing spudcans for jack-up rigs in a layered seabed with an interbedded strong-over-soft layer is challenging in the offshore industry due to possible punch-through failure. The methods currently used to predict punch-through failure mainly focus on generic spudcans, usually ignoring the geometric features of the spudcan. The aim of this study is to determine whether the punch-through potential of a generic spudcan is applicable to a cubic spudcan of a BH12# jack-up rig installed in dense sand overlying non-uniform clay. We conducted a series of large deformation finite element (LDFE) analyses on dense sand overlying non-uniform clay using a generic spudcan and a cubic spudcan. The thickness of the sand layer was also varied to cover a range of practical interest. The special cubic spudcan was found to be less likely to induce punch-through failure on sand-over-clay sediments compared with the corresponding generic spudcan. Herein, we propose a method to predict the degree of post-peak bearing reduction, which is a key measure of the severity of punch-through failure.

Keywords: jack-up rig; cubic spudcan; punch-through failure; dense sand overlying non-uniform clay; coupled Eulerian–Lagrangian

Citation: Zhao, J.; Zhang, Y.; Liu, L. On Cubic Spudcan Deep Penetration in Dense Sand Overlying Non-Uniform Clay. *J. Mar. Sci. Eng.* **2022**, *10*, 1607. https://doi.org/10.3390/jmse10111607

Academic Editor: Antoni Calafat

Received: 9 September 2022
Accepted: 27 October 2022
Published: 31 October 2022

Publisher's Note: MDPI stays neutral with regard to jurisdictional claims in published maps and institutional affiliations.

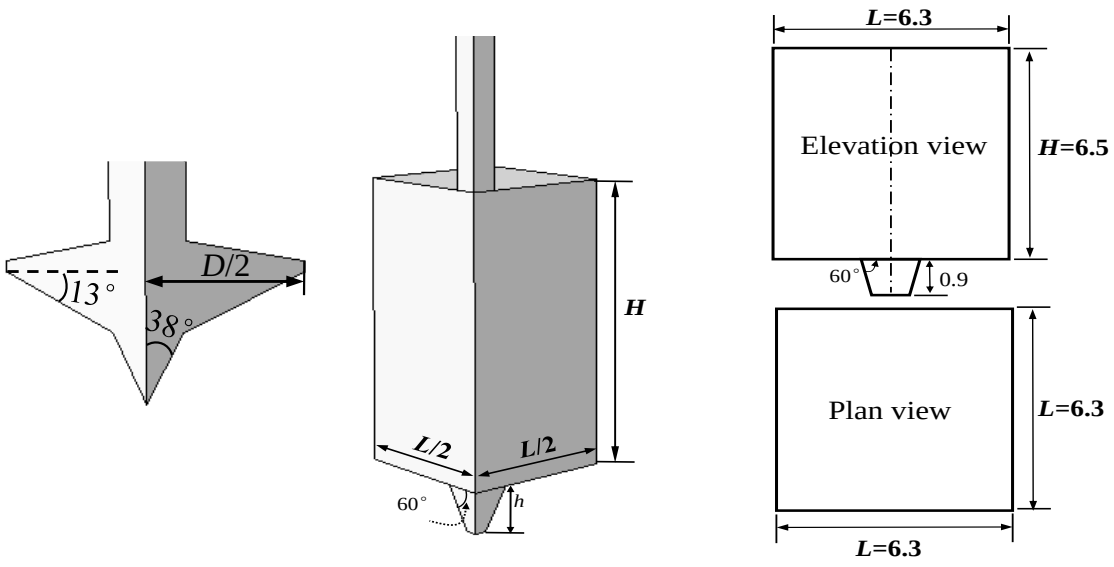
Copyright: © 2022 by the authors. Licensee MDPI, Basel, Switzerland. This article is an open access article distributed under the terms and conditions of the Creative Commons Attribution (CC BY) license (https://creativecommons.org/licenses/by/4.0/).

1. Introduction

Self-elevating jack-ups rigs have been widely used in shallow water to moderate water depths for offshore drilling and exploration, owing to their proven flexibility, mobility and cost-effectiveness [1]. During installation of a jack-up rig, a spudcan is loaded down by adding weight onto the legs in stages until it cannot sink any further under a given preload. In stratified sediments with interbedded strong-over-soft soil, punch-through failure of the spudcan foundation may occur, which is characterized by a sudden uncontrolled penetration into the underlying soft soils. Such a punch-through failure of a spudcan could lead to buckling of the leg and even toppling of the whole unit. An average rate of one punch-through accident per year was reported by Osborne and Paisley [2], corresponding to an economic loss of between USD 1 million and 10 million (per accident) due to rig damage and loss of drilling time. According to statistics reported by Hunt and Marsh [3], spudcan punch-through failure is the most hazardous of all geohazards associated with jack-up rigs, remaining prevalent in recent years, owing to the complex soil conditions encountered in the field.

Spudcan penetration in strong-over-soft sediments has been addressed by a number of researchers, with particular focus on the mechanism of punch-through failure and methods for predicting the (post) peak penetration resistance and the corresponding depth [4–20]. In addition, mitigating measures for possible punch-through failure of spudcans have been explored [21–25]. However, most research on punch-through failure

of spudcans mainly focus on generic spudcans (characterized by typical axisymmetric inverse conical characteristics; Figure 1a), although some modifications (e.g., varying bottom profile and holes through the footing) of generic spudcans have been explored [24].



(**a**) (**b**)

Figure 1. Schematic diagram of a quarter foundation: (**a**) generic spudcan; (**b**) cubic spudcan (m).

The BH12# jack-up rig is equipped with a special cubic spudcan (Figure 1b), which is nearly a cube, with a square cross section of L = 6.3 m, a height of H = 6.5 m (slightly larger than length of the cross-section side) and a 60° protruding spigot (with a tip height of 0.138H). To determine whether the same punch-through potential of a generic spudcan (Figure 1a) is applicable to a cubic spudcan (Figure 1b) in deeply penetrating dense sand-over-clay sediments, in this paper, we report the results of an extended investigation carried out through large deformation finite element (LDFE) analyses on dense sand overlying non-uniform clay using a generic (Figure 1a) and cubic spudcan (Figure 1b). The likelihood of punch-through failure of the generic spudcan and cubic spudcan is compared, with aim of evaluating the potential of punch-through of such a cubic spudcan (Figure 1b) in deeply penetrating dense sand-over-clay sediments.

2. Numerical Analysis

2.1. FE Modeling

LDFE analyses were performed in this study using the coupled Eulerian-Lagrangian (CEL) approach in ABAQUS/Explicit. The soil was modeled as an Eulerian domain of 4D in diameter to ensure that the boundaries were well outside the plastic zone (Figure 2). The Eulerian domain was discretized with 8-node linear Eulerian brick hexahedron elements with reduced integration, denoted as EC3D8R. A typical element size of 0.025D along the trajectory of the spudcan was adopted, as used in similar analyses [18,20,25]. The spudcan was simulated using C3D6 6-node linear brick wedge elements.

At top of the Eulerian domain, a void zone, which is initially defined with a void material, was included for potential soil movement. The lateral sides of the Eulerian domain were constrained by prescribing zero normal flow velocity, whereas the base of the Eulerian domain was constrained against flow in the vertical direction. To simulate the preloading process, the spudcan was constrained to move only in the vertical direction.

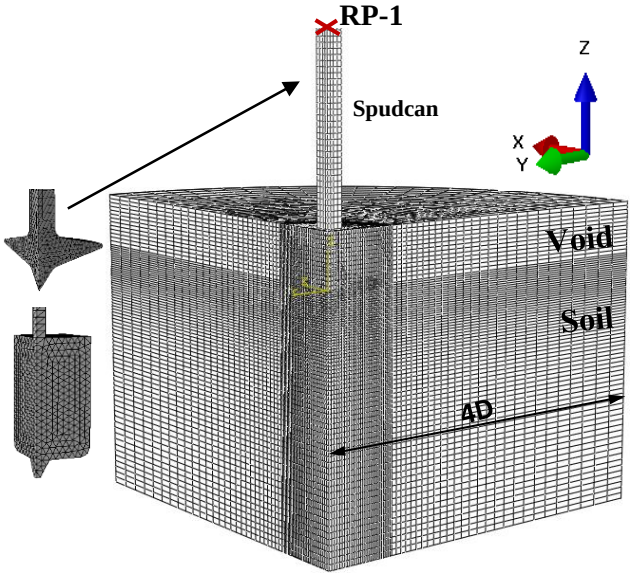


Figure 2. FE model of soil and the spudcan.

A value of 0.2 m/s was used in this study for the penetration rate of the spudcan foundation, similar to the rates adopted by Qiu and Henke [7] and Tho et al. [26]. For the clay soils, a value of 0.49 was used for the Poisson's ratio to ensure an undrained condition, whereas a value of 0.3 was adopted for the Poisson's ratio of the overlying dense sand. Owing to the minimal effects of the soil elastic stiffness on the ultimate failure load, typical values of E_{sand} = 50 MPa and E_{clay} = 350*s_{uc} were adopted for the Young's modulus of the sand and clay, respectively.

The interaction between the spudcan and the surrounding soils was imposed through the Eulerian–Lagrangian contact, which was described using the 'general contact' algorithm, which enforces the use of the penalty contact method. This contact method works without discrete contact elements. The 'general contact' algorithm with the finite-sliding formulation, which allows for arbitrary motion of the surface, is well-suited to simulate highly non-linear processes with large deformations. The frictional behavior between the soil and the spudcan was described using the linear-elastic, ideal plastic formulation proposed by Coulomb. For the dense sand-over-clay strata, the contact between the spudcan and the sand would be maintained during the full penetration. The frictional interaction between the spudcan and the sand was defined with a roughness factor of $\alpha = \frac{tan\delta}{tan\varphi'}$, where δ is the interface friction angle between the sand and the spudcan, and φ' is the friction angle of the sand. A roughness factor of α = 0.5, which is within the range of 0.3~0.5 suggested by SNAME guidelines [27], was adopted in this study.

2.2. Constitutive Models and Material Characteristics

The failure process that occurs along the slip surfaces in soils is progressive in nature because the plastic strain induced by loading is markedly non-uniform. Progressive failure has been observed in loading tests and centrifugal tests concerning footings on granular soils [28–30]. The progressive failure of a spudcan deeply penetrating in dense sand overlying clay was simulated in this study by incorporating variations of the shear strength parameters, such as the undrained shear strength (s_u) of the underlying clay and the mobilized friction angle (φ') and dilation angle (ψ') of the overlying sand.

2.2.1. Sand Layer

The modified Mohr–Coulomb (MMC) model proposed by Zhao et al. [20] was adopted in this study to simulate the behavior of the sand layer. The relationship between the mobilized shearing resistance angles (φ' and ψ') and the accumulated plastic shear

strain of sand layer (ξ_{sand}) is schematized in Figure 3. A peak strength (P_p) is followed by a gradual reduction to the critical state (P_c). The two thresholds (ξ_p and ξ_c) correspond to the peak and critical strength of the sand layer, respectively. Similar sand models have been adopted by Potts et al. [31], Hu et al. [12], Yapage et al. [32] and Zheng et al. [18].

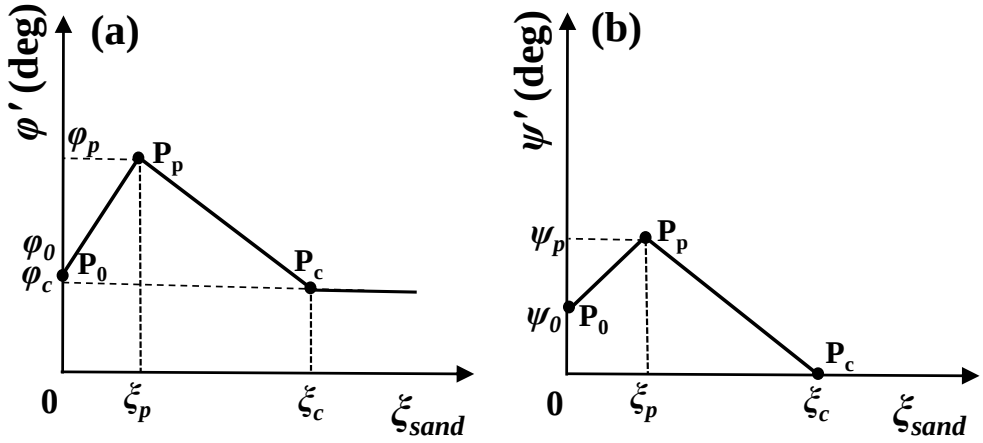


Figure 3. Variation of the friction and dilation angles of the modified Mohr–Coulomb model: (**a**) variation of friction angle; (**b**) variation of dilation angle.

The peak friction angle (φ_p) and corresponding dilation angle (ψ_p) of the upper dense sand layer at the peak resistance are determined with reference to the empirical strength–dilatancy correlations recommended by Bolton [33]:

$$\varphi_p - \varphi_c = mI_R \tag{1}$$

$$0.48\psi_p = \varphi_p - \varphi_c \tag{2}$$

$$I_R = I_D(10 - ln\, p') - 1 \tag{3}$$

where φ_c is the critical friction angle; m determines the enhancement of φ_p above the critical friction angle (φ_c) due to dilatancy, with a suggested value of m = 3 for triaxial (and general) stress conditions; and I_R ($0 \le I_R \le 4$) is a relative dilatancy index calculated as a function of both the relative density (I_D) and the mean effective stress applied on the soil (p').

The mean stress in the sand layer during large-footing penetration is mostly lower than 150 kPa [12,34]. For p' in Equation (3), a value of 150 kPa was suggested by Bolton [35]; for any p' value less than 150 kPa, the equation for I_R in Equation (3) is replaced with the following equation:

$$I_R = 5\, I_D - 1 \tag{4}$$

The accumulated plastic shear strain of sand layer (ξ_{sand}) (Figure 3) is defined as:

$$\xi_{sand} = \sum \left| \frac{\sigma_1 \Delta\varepsilon_1^{pl} + \sigma_2 \Delta\varepsilon_2^{pl} + \sigma_3 \Delta\varepsilon_3^{pl}}{\bar{\sigma}} \right| \tag{5}$$

where σ_i and $\Delta\varepsilon_i^{pl}$ (i = 1, 2, 3) are the stress components and incremental plastic strains measured from the start to the end of the current step, $\bar{\sigma}$ is the stress level index, and a value of 150 kPa [20] is adopted as noted previously, given that p' in overlying sand is usually less than 150 kPa.

2.2.2. Clay Layer

The intact undrained shear strength of the underlying non-uniform clay prior to any softening can be defined as $s_{u0} = s_{um} + kz$, where s_{um} is the clay strength at the sand/clay interface, k is the strength gradient and z represents the depth of the underlying clay. Strain softening was simulated using an extended Tresca model in accordance

with the method proposed by Einav and Randolph [36]. Considering the negligible elastic shear strain compared with the plastic shear strain in the LDFE analysis, the accumulated shear strain (ξ_{clay}) for the underlying clay is defined as:

$$\xi_{clay} = \sum \left| \Delta\varepsilon_1^{pl} - \Delta\varepsilon_3^{pl} \right| \quad (6)$$

where $\Delta\varepsilon_1^{pl}$ and $\Delta\varepsilon_3^{pl}$ are the increments of maximum and minimum principal plastic strains, respectively.

The current undrained shear strengths (s_{uc}) at the integration points are updated at the beginning of each time step as:

$$s_{uc} = (\delta_{rem} + (1 - \delta_{rem}) e^{-3\xi_{clay}/\xi_{95}}) s_{u0} \quad (7)$$

where δ_{rem} is the strength ratio of soil between fully remolded and intact states (the inverse of the sensitivity (S_t); a value of S_t = 3 adopted, which falls within the typical range of S_t from 2 to 5 for marine clays [37–39]); ξ_{95} represents the value of ξ_{clay} required for soil to undergo 95% remolding (a typical value of ξ_{95} = 12 within the range of 10 to 50 for marine clays was used) [40].

3. Validation against Centrifuge Test Data

To validate the numerical model, four centrifuge tests were numerically recalculated for spudcan deep penetration in dense sand-over-clay deposits with (test FS13) or without (tests H3C14, T1 and D1SP70a) a first-layer clay [4,8,10,13]. The soil parameters used in the centrifuge tests are listed in Table 1. In tests T1, H3C14 and D1SP70a, a dense sand layer (H3C14: silica sand with I_D = 74%; T1: silica sand with I_D = 85% and D1SP70a: silica sand with I_D = 92%) overlay a non-uniform clay with strength gradients of 1.2 kPa/m, 1.56 kPa/m and 2.1 kPa/m were used. Test FS13 was carried out for a dense sand layer (silica sand with I_D = 89%) sandwiched between two non-uniform clay layers with strength gradients of k = 1.2 kPa/m and 2.1 kPa/m, respectively.

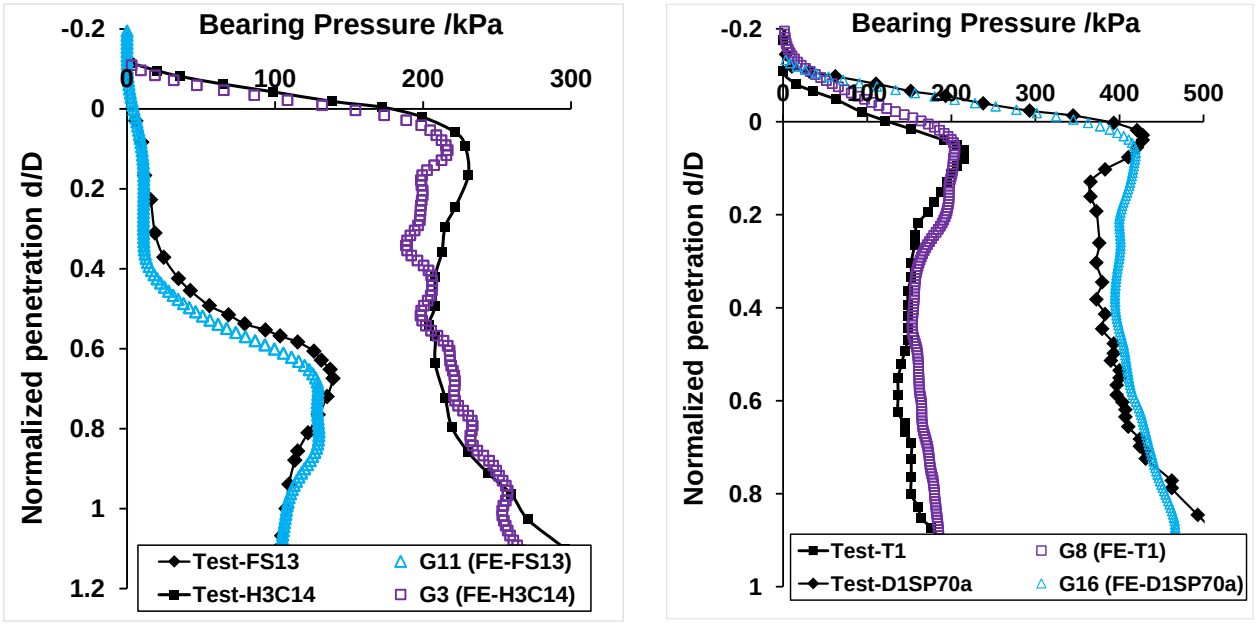
For tests FS13, H3C14, T1 and D1SP70a, corresponding LDFE analyses were conducted (G11, G3, G8 and G16, respectively (Table 2)); the measured and computed penetration resistance profiles are compared in Figure 4. The parameters used in the LDFE analyses for progressive failure of the sand layer are listed in Table 2. The numerical predictions show reasonable agreement with the corresponding centrifuge test results in terms of key features of the penetration resistance profile, including the depth and magnitude of the peak resistance in the sand layer.

Table 1. Soil properties used in centrifuge tests

Test	**1st layer**				**2nd layer**				
T1	$t1$(m)	I_D (%)	φ_c (°)	γ' (kN/m³)	s_{um} (kPa)	γ' (kN/m³)	k (kPa/m)		Teh et al. [4]
(D = 6 m)	3	85	34	10.8	6.0	6.5	1.2		
D1SP70a	1st layer				2nd layer				
(D = 14 m)	$t1$(m)	I_D (%)	φ_c (°)	γ' (kN/m³)	s_{um} (kPa)	γ' (kN/m³)	k (kPa/m)		Lee et al. [8]
	6.2	92	31	11.0	17.7	7.5	2.1		
H3C14	1st layer				2nd layer				
(D = 8 m)	$t1$(m)	I_D (%)	φ_c (°)	γ'(kN/m³)	s_{um} (kPa)	γ' (kN/m³)	k (kPa/m)		Hu [13]
	3.03	74	31	10.6	11.31	6.5	1.51		
	1st layer				2nd layer				
	$t1$(m)	s_{um} (kPa)	γ' (kN/m³)	$k1$ (kPa/m)	$t2$(m)	I_D (%)	φ (°)	γ' (kN/m³)	
FS13	3.7	0.5	6.5	0.75	2	89	34	10.0	Hossain [10]
(D = 6 m)	3rd layer								
	$t3$(m)	s_{um} (kPa)	γ' (kN/m³)	$k3$ (kPa/m)					
	20.8	4.775	6.5	0.75					

Table 2. Summary of LDFE analyses.

Test	Serial Number	Name	Sand				Clay	
			t_s (m)	D (L) (m)	ξ_p	ξ_c	s_{um} (kPa)	k (kPa/m)
H3C14	1	G1	1.2	8	0.01	0.4	11.31	1.51
		S1		7.09				
	2	G2	2	8				
		S2		7.09				
	3	**G3**	**3.03**	8				
		S3		7.09				
	4	G4	4	8				
		S4		7.09				
T1	5	G5	0.9	6	0.01	0.4	6	1.2
		S5		5.32				
	6	G6	1.5	6				
		S6		5.32				
	7	G7	2.1	6				
		S7		5.32				
	8	**G8**	**3**	6				
		S8		5.32				
FS13	9	G9	0.9	6	0.01	0.23	4.775	0.75
		S9		5.32				
	10	G10	1.5	6				
		S10		5.32				
	11	**G11**	**2**	6				
		S11		5.32				
	12	G12	3	6				
		S12		5.32				
D1SP70a	13	G13	2.1	14	0	0.1	17.7	2.1
		S13		12.41				
	14	G14	3.5	14				
		S14		12.41				
	15	G15	4.9	14				
		S15		12.41				
	16	**G16**	**6.2**	14				
		S16		12.41				



(**a**) (**b**)

Figure 4. Comparison of resistance profiles of generic spudcans from the centrifuge test and numerical analysis: (**a**) test H3C14 and FS13; (**b**) test T1 and D1SP70a.

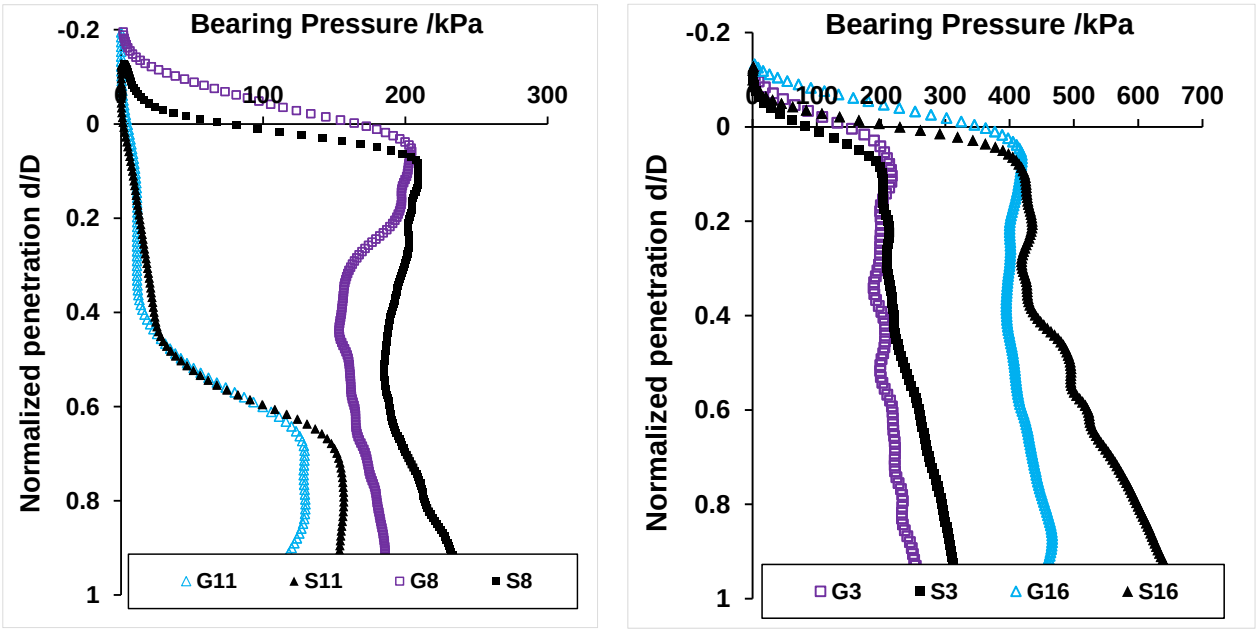
For the post-peak rate of reduction in the sand layer, the computed profile values are lower than the measured values, especially for test D1SP70a, which may be partly due to the simplification in the sand model used. However, the accuracy of the present numerical model is acceptable, as the aim of this study was to determine whether the punch-through potential for a generic spudcan (Figure 1a) is applicable to a special cubic spudcan equipped with a BH12# jack-up rig, as reflected by the differences in the resistance profiles of the generic and cubic spudcans (Figure 1).

4. Potential of Punch-Through Failure of the Cubic Spudcan

4.1. Penetration Resistance Profile

To compare performance of the generic and cubic spudcans (Figure 1) in deeply penetrating dense sand overlying non-uniform clay, LDFE analyses were conducted using two distinct generic and cubic spudcans. The length of the cross-section side of the cubic spudcan ($L = \frac{D}{2}\sqrt{\pi}$) (Figure 1) was adopted to obtain the same area with the largest cross-section of corresponding generic spudcan. Table 2 shows a summary of the LDFE analyses conducted in this study.

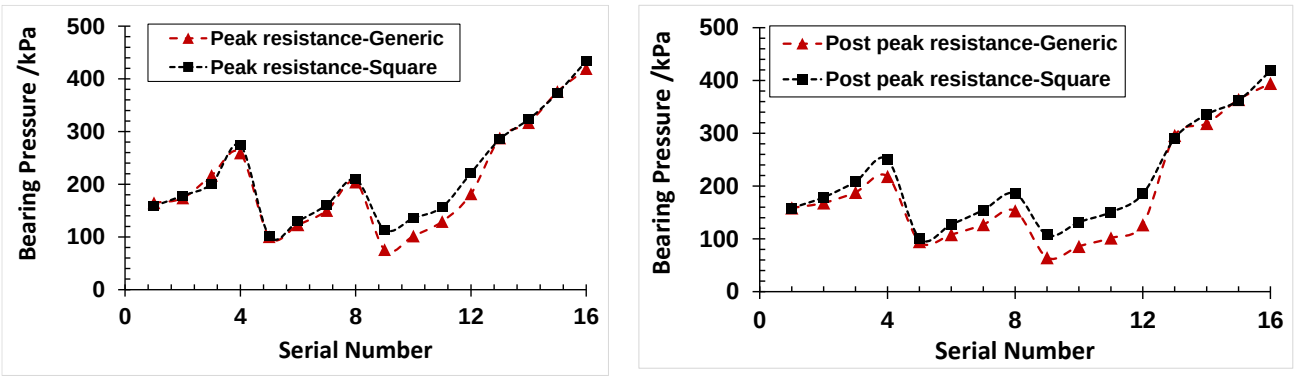
The penetration resistance profiles of the cubic spudcan with the same cross-section area as the corresponding generic spudcan were numerically calculated using the soil profiles from tests T1, FS13, H3C14 and D1SP70a. Figure 5 shows a comparison of the penetration resistance profiles of the generic and cubic spudcans. Compared with the corresponding generic spudcan, the post-peak rate of reduction at punch-through of the cubic spudcan is lower, indicating a lower risk of punch-through failure.



(a) (b)

Figure 5. Comparison of resistance profiles of generic and cubic spudcans: (**a**) test T1 and FS13; (**b**) test H3C14 and D1SP70a.

With respect to the performance of the cubic spudcan on dense sand-over-clay sediments, the effects of sand thickness (t/D) on the potential for punch-through failure were further analyzed. The peak and post-peak penetration resistance of the generic and corresponding cubic spudcan are compared in Figure 6. Little difference in peak penetration resistance is shown between the generic and cubic spudcan, whereas the post-peak resistance of the cubic spudcan is higher than that of the corresponding generic spducan, especially for tests T1, FS13 and H3C14.



(a) (b)

Figure 6. Comparison of the peak and post-peak resistance of the generic and cubic spudcans: (**a**) peak resistance; (**b**) post-peak resistance.

Because the ratio of post-peak resistance to peak resistance ($q_{post\text{-}peak}/q_{peak}$) is one of the key factors indicating the severity of punch-through failure, the values of $q_{post\text{-}peak}/q_{peak}$ for tests H3C14, T1, FS13 and D1SP70a were calculated to further explore differences in peak and post-peak resistance between the generic and cubic spudcans. Figure 7 shows variations in $q_{post\text{-}peak}/q_{peak}$ with normalized thickness of the sand layer t/D (L) for tests H3C14, T1, FS13 and D1SP70a. Overall, the values of $q_{post\text{-}peak}/q_{peak}$ for the cubic spudcan are higher than

those for the corresponding generic spudcan, although limited differences were observed in test D1SP70a. The cubic spudcan may mitigate the potential of punch-through failure to a certain extent relative to the corresponding generic spudcan.

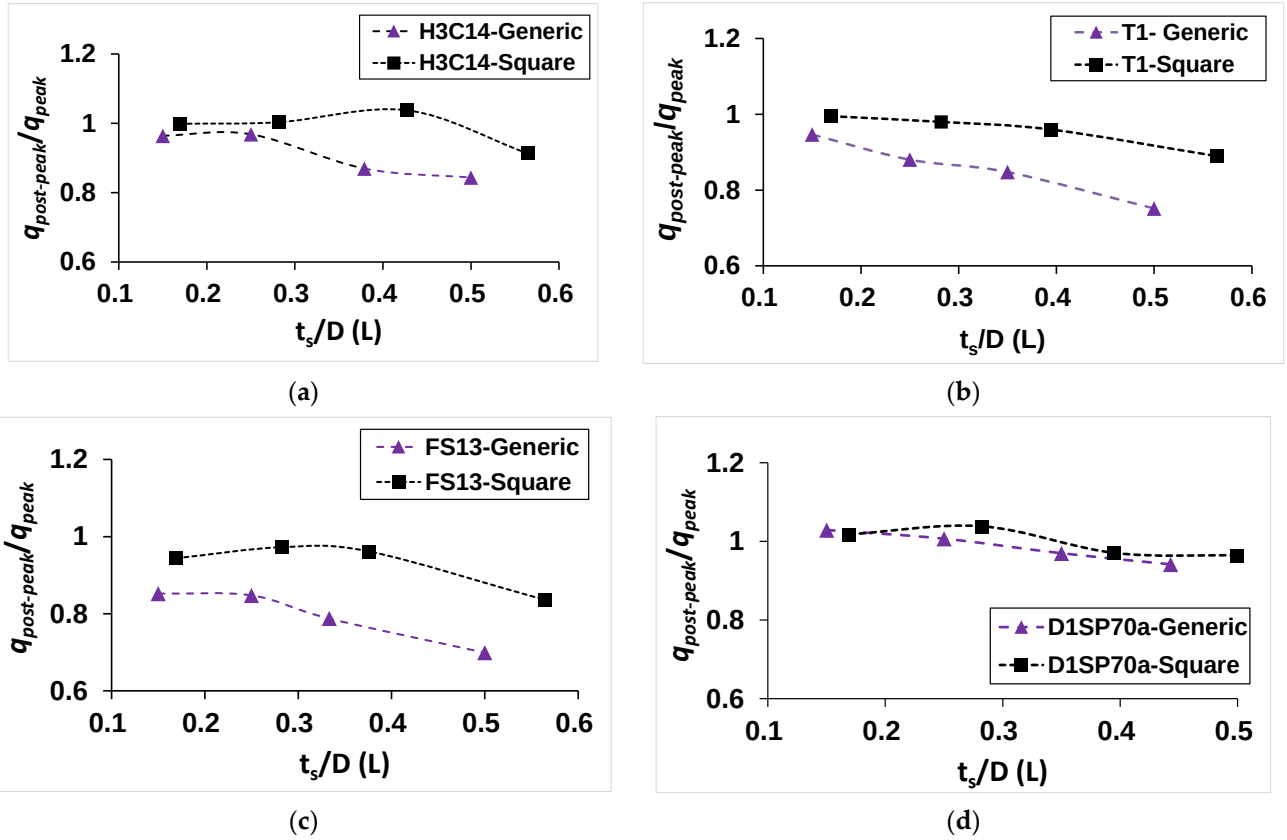


Figure 7. Effect of sand layer thickness on $q_{post\text{-}peak}/q_{peak}$: (**a**) test H3C14; (**b**) test T1; (**c**) test FS13; and (**d**) test D1SP70a.

4.2. Degree of the Post-Peak Bearing Reduction

To quantify severity of punch-through failure, the degree of post-peak bearing reduction ($\lambda = {}^{\Delta[q_u/(d/D)]}/_{s_{u,avg}}$) was calculated based on results of the LDFE analyses (Table 2) conducted in this study. The values of λ for both the generic and cubic spudcan foundations (Figure 1) are shown in Figure 8. The values of λ for the cubic the spudcan are generally higher than those of the corresponding generic spudcan, indicating a lower probability of punch-through failure.

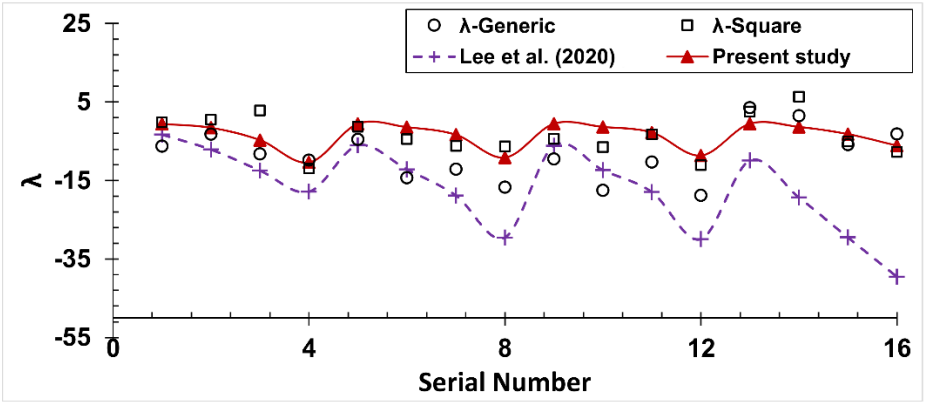


Figure 8. Comparison of degree of post-peak gradient (λ) predictions.

The λ prediction method proposed by Lee et al. [25] for generic spudcans was used in this study. Compared with the λ values obtained in LDFE analyses, as shown in Figure 8, the values of λ for the cubic spudcan are underestimated, which may be partially due to the differences in punch-through failure between the generic and cubic spudcans, as addressed above. Based on the LDFE results obtained in this study for the cubic spudcan, the following method is proposed for prediction of λ for cubic spudcans:

$$\lambda = -21\left(\frac{t_s}{L}\right)^3 \ln\left(6.14 + 1.5\frac{kL}{s_{u,avg}}\right)(I_D)^{-1} + 1.4 \quad (8)$$

where t_s is the thickness of sand layer, L is the length of the cross-section side of the cubic spudcan, k is the rate of increase in undrained shear strength with depth within clay layer and $s_{u,avg}$ is the undrained shear strength of clay averaged over 0.5 D(L).

5. Concluding Remarks

The deep penetration of generic and cubic spudcans in sediments with interbedded dense sand overlying non-uniform clay were numerically simulated in this study, with the aim of determining whether the potential of punch-through failure of a generic spudcan is applicable to a nearly cubic spudcan with a BH12# jack-up rig. A series of LDFE analyses were conducted using a modified Mohr–Coulomb (MMC) model for progressive failure of the interbedded dense sand and an extended Tresca model for strain softening of the clay. The FE model was validated against results from four centrifuge tests for spudcan deep penetration in a dense sand-over-clay deposit with or without a first-layer clay, and reasonable agreement was obtained.

Comparison of the resistance profiles, peak and post-peak resistances revealed few differences in peak penetration resistance between the generic and cubic spudcans, whereas post-peak resistances of the cubic spudcan were higher than those of the corresponding generic spducan. Variations in $q_{post\text{-}peak}/q_{peak}$ with normalized thickness of the sand layer t/D (L) were further comparatively analyzed for generic and cubic spudcans. The values of $q_{post\text{-}peak}/q_{peak}$ for the cubic spudcan were found to be higher than those of the corresponding generic spudcan. Therefore, compared with a generic spudcan, a cubic spudcan may be less likely to undergo punch-through failure on dense sand-over-clay deposits, possibly as a consequence of less soil backflow on top of the cubic spudcan. We also proposed a prediction method herein is for the degree of post-peak bearing reduction (λ) to quantify the severity of punch-through failure.

Author Contributions: Conceptualization, J.Z.; methodology, J.Z.; software, J.Z.; validation, J.Z.; formal analysis, J.Z.; investigation, J.Z., Y.Z. and L.L.; resources, J.Z., L.L. and Y.Z.; data curation, J.Z. and Y.Z.; writing—original draft preparation, J.Z.; writing—review and editing, J.Z., Y.Z. and L.L.; visualization, J.Z.; supervision, J.Z.; project administration, J.Z.; funding acquisition, J.Z. All authors have read and agreed to the published version of the manuscript.

Funding: This research was funded by the National Natural Science Foundation of China (grant no. 51609201) and the Natural Science Basic Research Program of Shaanxi Province (grant no. 2020JQ-784).

Institutional Review Board Statement: Not applicable.

Informed Consent Statement: Not applicable.

Data Availability Statement: Not applicable.

Acknowledgments: The authors would like to thank the editors and reviewers for their many constructive suggestions and comments that helped improve the quality of the paper.

Conflicts of Interest: The authors declare no conflict of interest.

Abbreviations

d	penetration depth of the spudcan base (lowest point at largest section)
D	diameter of the generic spudcan at the largest section
H	height of the cubic spudcan
I_D	relative density of sand
k	strength gradient of clay (in kPa/m)
L	length of the cross-section of the cubic spudcan
q_{peak}, $q_{post\text{-}peak}$	peak and post-peak penetration resistance of the spudcan
s_{um}	intact undrained shear strength on top of clay
s_{u0}	intact undrained shear strength of soil
s_{uc}	current undrained shear strength of soil accounting for strain rate and softening
$s_{u,avg}$	undrained shear strength of clay averaged over 0.5D(L)
$t1$, $t2$, $t3$	thickness of the first, second layer and third layer
t_s	thickness of the sand layer
z	depth of the underlying clay
α	roughness factor of the interaction between the spudcan and sand
γ'	effective unit weight of soil
$\varphi_0, \varphi_p, \varphi_c$	initial, peak and critical friction angle of sand
ψ_0, ψ_p	initial and peak dilation angle of sand
ξ_{sand}, ξ_{clay}	accumulated plastic shear strain of sand and clay
ξ_p, ξ_c	thresholds corresponding to the peak and critical strength of sand, respectively
σ_i (i = 1, 2, 3)	stress components measured from the start to end of the current step
$\Delta\varepsilon_i^{pl}$(i = 1, 2, 3)	incremental plastic strains measured from the start to end of the current step
λ	degree of post-peak bearing reduction

References

1. Randolph, M.; Cassidy, M.; Gourvenec, S.; Erbrich, C. Challenges of offshore geotechnical engineering. In Proceedings of the 16th International Conference on Soil Mechanics and Geotechnical Engineering, Osaka, Japan, 12–15 September 2005; pp. 123–176.
2. Osborne, J.J.; Paisley, J.M. S E Asia Jack-up Punch-throughs: The Way Forward. In Proceedings of the International Conference on Offshore Site Investigation and Geotechnics Sustainability and Diversity, London, UK, 26–28 November 2002; pp. 301–306.
3. Hunt, R.J.; Marsh, P.D. Opportunities to Improve the Operational and Technical Management of Jack-up Deployments. *Mar. Struct.* **2004**, *17*, 261–273.
4. Teh, K.L.; Cassidy, M.J.; Leung, C.F.; Chow, Y.K.; Randolph, M.F.; Quah, C. Revealing the bearing capacity mechanisms of a penetrating spudcan through sand overlying clay. *Geotechnique* **2008**, *58*, 793–804.
5. Teh, K.L.; Leung, C.F.; Chow, Y.K.; Cassidy, M.J. Centrifuge Model Study of Spudcan Penetration in Sand Overlying Clay. *Geotechnique* **2010**, *60*, 825–842.
6. Qiu, G.; Henke, S.; Grabe, J. Application of a coupled Eulerian-Lagrangian approach on geomechanical problems involving large deformations. *Comput. Geotech.* **2011**, *38*, 30–39.
7. Qiu, G.; Grabe, J. Numerical investigation of bearing capacity due to spudcn penetration in sand overlying clay. *Can. Geotech. J.* **2012**, *49*, 1393–1407.
8. Lee, K.K.; Cassidy, M.J.; Randolph, M.F. Bearing capacity on sand overlying clay soils: Experimental and finite element investigation of potential punch-through failure. *Geotechnique* **2013**, *63*, 1271–1284.
9. Lee, K.K.; Randolph, M.F.; Cassidy, M.J. Bearing capacity on sand overlying clay soils: A simplified conceptual model. *Geotechnique* **2013**, *63*, 1285–1297.
10. Hossain, M.S. Experimental investigation of spudcan penetration in multi-layer clays with interbedded sand layers. *Geotechnique* **2014**, *64*, 258–277.
11. Hu, P.; Wang, D.; Cassidy, M.J.; Stanier, S.A. Predicting the resistance profile of a spudcan penetrating sand overlying clay. *Can. Geotech. J.* **2014**, *51*, 1151–1164.
12. Hu, P.; Wang, D.; Stanier, S.A.; Cassidy, M.J. Assessing the punch-through hazard of a spudcan on sand overlying clay. *Geotechnique* **2015**, *65*, 883–896.
13. Hu, P. Predicting Punch-Through Failure of a Spudcan on Sand Overlying Clay. Ph.D. Thesis, University of Western Australia, Crawley, Australia, 2015.
14. Hu, P.; Cassidy, M.J. Predicting jack-up spudcan installation in sand overlying stiff clay. *Ocean Eng.* **2017**, *146*, 246–256. https://doi.org/10.1016/j.oceaneng.2017.09.046.
15. Zhao, J.; Jang, B.S.; Duan, M.L. Investigation of Spudcan continuous penetration in multi-layer sediments with interbedded sand-overlaid-clay soil profile. In Proceedings of the 25th International Offshore and Polar Engineering Conference, Kona, HI, USA, 21–26 June 2015.

16. Zhao, J.; Jang, B.S.; Duan, M.L.; Song, L.S. Simplified numerical prediction of the penetration resistance profile of spudcan foundation on sediments with interbedded medium-loose sand layer. *Appl. Ocean Res.* **2016**, *55*, 89–101.
17. Zhao, J.; Jang, B.S.; Duan, M.L. On spudcan deep penetration using Eulerian finite element in multi-layer sediments: Soil plug mechanism. *Ships Offshore Struct.* **2017**, *12*, 715–721.
18. Zheng, J.; Hossain, M.S.; Wang, D. Numerical investigation of spudcan penetration in multi-layer deposits with an interbedded sand layer. *Geotechnique* **2017**, *67*, 1050–1066. https://doi.org/10.1680/jgeot.16.P.110.
19. Ullah, S.N.; Hu, Y. Peak punch-through capacity of spudcan in sand with interbedded clay: Numerical and analytical modelling. *Can. Geotech. J.* **2017**, *54*, 1071–1088. https://doi.org/10.1139/cgj-2016-0597.
20. Zhao, J.; Jang, B.S.; Duan, M.L.; Liang, C. A finite element approach for predicting the full resistance profile of a spudcan deeply penetrating in dense sand overlying clay. *Appl. Ocean Res.* **2019**, *87*, 155–164.
21. Hossain, M.S.; Hu, Y.; Ekaputra, D. Skirted foundation to mitigate spudcan punch-through on sand-over-clay. *Geotechnique* **2014**, *64*, 333–340.
22. Hu, P.; Stanier, S.A.; Wang, D.; Cassidy, M.J. Effect of footing shape on penetration in sand overlying clay. *Int. J. Phys. Model. Geotech.* **2016**, *16*, 119–133.
23. Li, Y.P.; Liu, Y.; Lee, F.H.; Goh, S.H.; Zhang, X.Y.; Wu, J.F. Effect of sleeves and skirts on mitigating spudcan punch-through in sand overlying normally consolidated clay. *Geotechnique* **2019**, *69*, 283–296. https://doi.org/10.1680/jgeot.17.P.085.
24. Lee, J.M.; Hossain, M.S.; Hu, P.; Kim, Y.H.; Cassidy, M.J.; Hu, Y.; Park, S.G. Effect of spudcan shape on mitigating punch-through in sand-over-clay. *Int. J. Phys. Model. Geotech*. **2019**, *20*, 150–163. https://doi.org/10.1680/jphmg.18.00072.
25. Lee, J.M.; Kim, Y.H.; Hossain, M.S.; Cassidy, M.J.; Hu, Y.; Park, S.G. Mitigating punch-through on sand-over-clay using skirted foundations. *Ocean Eng*. **2020**, *201*, 107133. https://doi.org/10.1016/j.oceaneng.2020.107133.
26. Tho, K.K.; Leung, C.F.; Chow, Y.K.; Swaddiwudhipong, S. Eulerian Finite-Element Technique for Analysis of Jack-Up Spudcan Penetration. *Int. J. Geomech.* **2012**, *12*, 64–73.
27. SNAME. *Guidelines for Site Specific Assessment of Mobile Jack-Up Units*; T & R Bulletin 5-5 and 5-5A; SNAME: Houston, TX, USA, 2008.
28. Yamaguchi, H.; Kimura, T.; Fujii, N. On the influence of progressive failure on the bearing capacity of shallow foundation in dense sand. *Soils Found*. **1976**, *16*, 11–22.
29. Aiban, S.A.; Znidarcic, D. Centrifugal modelling of bearing capacity of shallow foundations on sand. *J. Geotech. Eng*. **1995**, *121*, 704–712. https://doi.org/10.1061/(ASCE)0733-9410(1995)121:10(704).
30. Perkins, S.W.; Madson, C.R. Bearing capacity of shallow foundations on sand: A relative density approach. *J. Geotech. Geoenviron. Eng*. **2000**, *126*, 521–530.
31. Potts, D.M.; Dounias, G.T.; Vaughan, P.R. Finite element analysis of progressive failure of carsington embankment. *Geotechnique* **1990**, *40*, 79–101.
32. Yapage, N.; Liyanapathirana, D.; Poulos, H.; Kelly, R.; Leo, C. Numerical modeling of geotextile-reinforced embankments over deep cement mixed columns incorporating strain softening behavior of columns. *Int. J. Geomech*. **2015**, *15*, 04014047-1–04014047-18.
33. Bolton, M.D. The strength and dilatancy of sands. *Geotechnique* **1986**, *36*, 65–78.
34. White, D.J.; Teh, K.L.; Leung, C.F.; Chow, Y.K. A comparison of the bearing capacity of flat and conical circular foundations on sand. *Geotechnique* **2008**, *58*, 781–792. https://doi.org/10.1680/geot.2008.3781.
35. Bolton, M.D. The strength and dilatancy of sands, Discussion. *Geotechnique* **1987**, *37*, 219–226.
36. Einav, I.; Randolph, M.F. Combining upper bound and strain path methods for evaluating penetration resistance. *Int. J. Numer. Methods Eng.* **2005**, *63*, 1991–2016.
37. Kvalstad, T.J.; Nadim, F.; Harbitz, C.B. Deepwater geohazards: Geotechnical concerns and solutions. In Proceedings of the Offshore Technology Conference, Houston, TX, USA, 30 April–3 May 2001.
38. Andersen, K.H.; Jostad, H.P. Shear strength along inside of suction anchor skirt wall in clay. In Proceedings of the Offshore Technology Conference, Houston, TX, USA, 3–6 May 2004.
39. Randolph, M.F. Characterization of soft sediments for offshore applications. Keynote Lecture. In Proceedings of the 2nd International Conference on Site Characterization, Porto, Portugal, 19–22 September 2004; pp. 209–232.
40. Zhou, H.; Randolph, M.F. Resistance of full-flow penetrometers in rate-dependent and strain-softening clay. *Geotechnique* **2009**, *59*, 79–86. https://doi.org/10.1680/geot.2007.00164.